RESEARCH ARTICLE

Carbothermal shock synthesis of high-entropy-alloy nanoparticles

Yonggang Yao[1,*], Zhennan Huang[2,*], Pengfei Xie[3,*], Steven D. Lacey[1,*], Rohit Jiji Jacob[4], Hua Xie[1], Fengjuan Chen[1], Anmin Nie[2], Tiancheng Pu[3], Miles Rehwoldt[4], Daiwei Yu[5], Michael R. Zachariah[4], Chao Wang[3,†], Reza Shahbazian-Yassar[2,†], Ju Li[5,†], Liangbing Hu[1,†]

[1]*Department of Materials Science and Engineering, University of Maryland, College Park, MD 20742, USA.*

[2]*Department of Mechanical and Industrial Engineering, University of Illinois at Chicago (UIC), Chicago, IL 60607, USA.*

[3]*Department of Chemical and Biomolecular Engineering, Johns Hopkins University, Baltimore, MD 21218, USA.*

[4]*Department of Chemical and Biomolecular Engineering and Chemistry and Biochemistry, University of Maryland, College Park, MD 20742, USA.*

[5]*Department of Nuclear Science and Engineering, Department of Materials Science and Engineering, and Department of Electrical Engineering and Computer Science, Massachusetts Institute of Technology, Cambridge, MA 02139, USA.*

†Corresponding author. Email: binghu@umd.edu (L.H.); rsyassar@uic.edu (R.S.-Y.); liju@mit.edu (J.L.); chaowang@jhu.edu (C.W.)

* These authors contributed equally to this work.

Science 30 Mar 2018:
Vol. 359, Issue 6383, pp. 1489-1494
DOI: 10.1126/science.aan5412

Group Meeting, 29-06-18
Paper Presentation

- Ankit Nagar

Background

- MMNPs applications: catalysis, energy storage, bio/plasmonic imaging
- Current approaches to synthesize MMNPs: wet chemistry syntheses. But alloy compositions do not exceed three elements
- Melt processing method: Useful for 5 or more elements to create bulk materials useful as structural materials

Challenges:

- Limited family of HEAs because of difficulty in mixing elements with different physical and chemical properties, as well as cooling rate constraints.
- Downsizing HEAs to nanoscale is daunting using conventional alloying methods.
- Lack of precise control over elemental composition, particle size and phase

Relevance

Towards High-Entropy-Alloy Clusters by subsequent doping:

$Ag_{25}(DMBT)_{18}$ -> $PtAg_{24}(DMBT)_{18}$, $PdAu_xAg_{24-x}(DMBT)_{18}$, $PtAu_xAg_{24-x}(DMBT)_{18}$ .... or $Au_{12}Ag_{13}(DMBT)_{18}$

Introduction

- The controllable incorporation of multiple immiscible elements into a single nanoparticle- unexplored
- Challenging using conventional techniques
- Eight dissimilar elements -> single-phase solid solution NPs (high-entropy-alloy NPs)
- Procedure: Precursor metal salt mixtures loaded onto carbon supports -> thermal shock [temperature ~2000K, 55-ms duration, rate of ~10^5 K per second]
- **CTS advantages:**

1. narrow-size distributed MMNPs,
2. uniformly dispersed across carbon support
3. no coarsening at higher temperatures

Precursors	Chemical reduction potential [V]	Physical decom-position T [K]	Metals	Atomic Radius [Å]	Melting point [K]	Boiling point [K]	Room-T structure
H_2PtCl_6	0.68, 0.73, 1.18	573, 653, 853	Pt	1.39	2041	4098	FCC
$PdCl_2$	0.95	952	Pd	1.37	1828	3236	FCC
$NiCl_2$	-0.25	>1073	Ni	1.24	1728	3186	FCC
$FeCl_3$	0.77, -0.44	553, 588	Fe	1.26	1811	3134	BCC
$CoCl_2$	-0.28	>873	Co	1.25	1768	3200	HCP
$HAuCl_4$	1.5	527	Au	1.44	1337	3129	FCC
$CuCl_2$	0.34	1266	Cu	1.28	1358	3200	FCC
$SnCl_2$	-0.14	896	Sn	1.40	505	2875	tetragonal

Physio-chemical properties of the elemental precursor salts used and corresponding metals.

Results
CTS Synthesis of HEA NPs on Carbon Supports

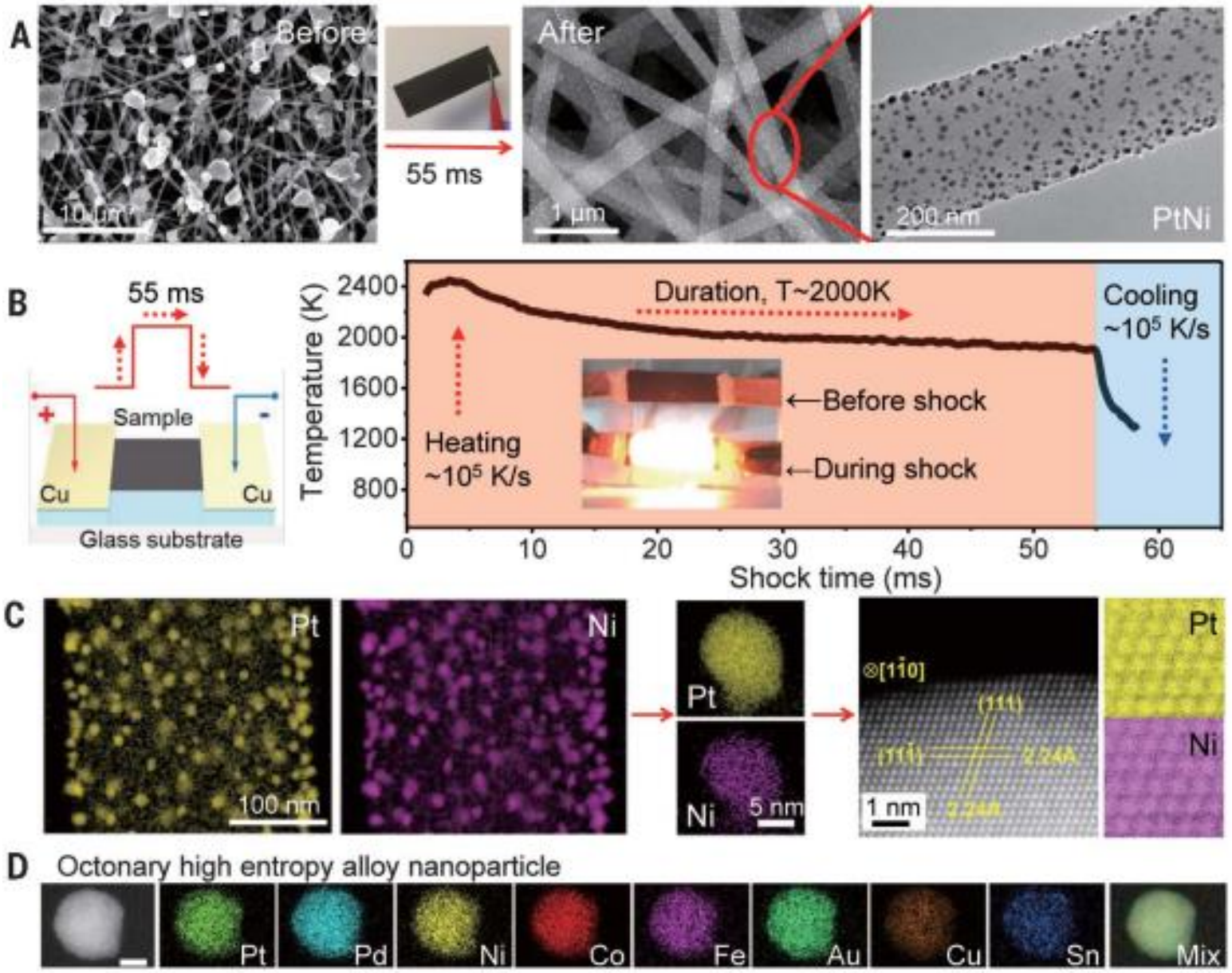

Fig. 1. CTS synthesis of HEA-NPs on carbon supports. (A) Microscopy images of microsized precursor salt particles on the carbon nanofiber (CNF) support before thermal shock, as well as the synthesized, well-dispersed (PtNi) nanoparticles after CTS. (B) Sample preparation and the temporal evolution of temperature during the 55-ms thermal shock. (C) Low-magnification and single-particle elemental maps, an HAADF image, and corresponding atomic maps for a binary PtNi alloy. (D) Elemental maps of an HEA-NP composed of eight dissimilar elements (Pt, Pd, Ni, Co, Fe, Au, Cu, and Sn). Scale bar, 10 nm.

Results
Elemental Characterization of HEA NPs

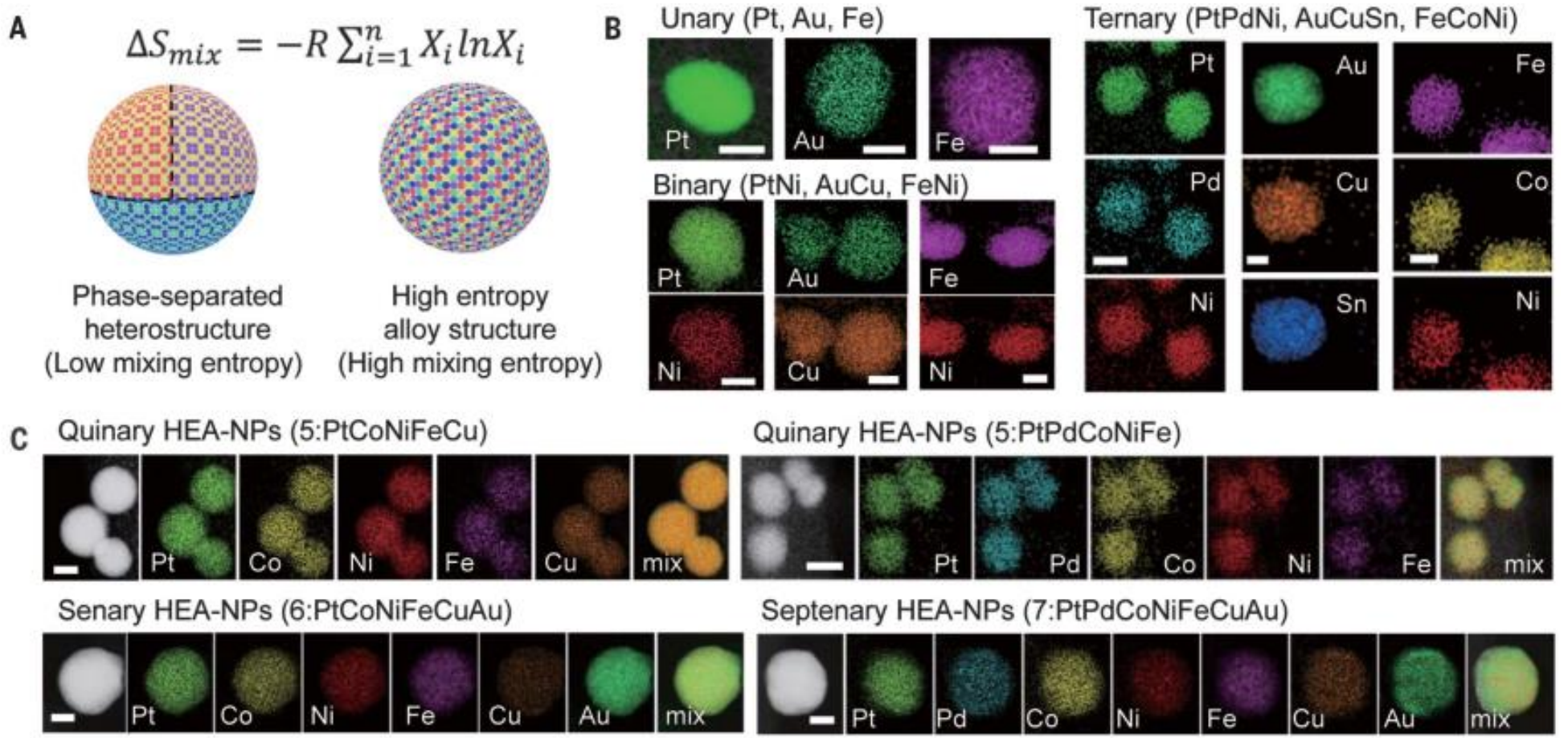

Fig. 2. Elemental characterization of HEA-NPs. (A) Schematic comparison of phase-separated heterostructures synthesized by a conventional slow reduction procedure (slow kinetics) versus solid-solution HEA-NPs synthesized by the CTS method (fast kinetics). (B) STEM elemental maps of unary (Pt, Au, and Fe), binary (PtNi, AuCu, and FeNi), and ternary (PtPdNi, AuCuSn, and FeCoNi) nanoalloys. Scale bar, 5 nm. (C) HAADF images and STEM elemental maps of HEA-NPs: quinary (PtFeCoNiCu and PtPdCoNiFe), senary (PtCoNiFeCuAu), and septenary (PtPdCoNiFeCuAu). Scale bar, 10 nm.

Results
Elemental Characterization of HEA NPs

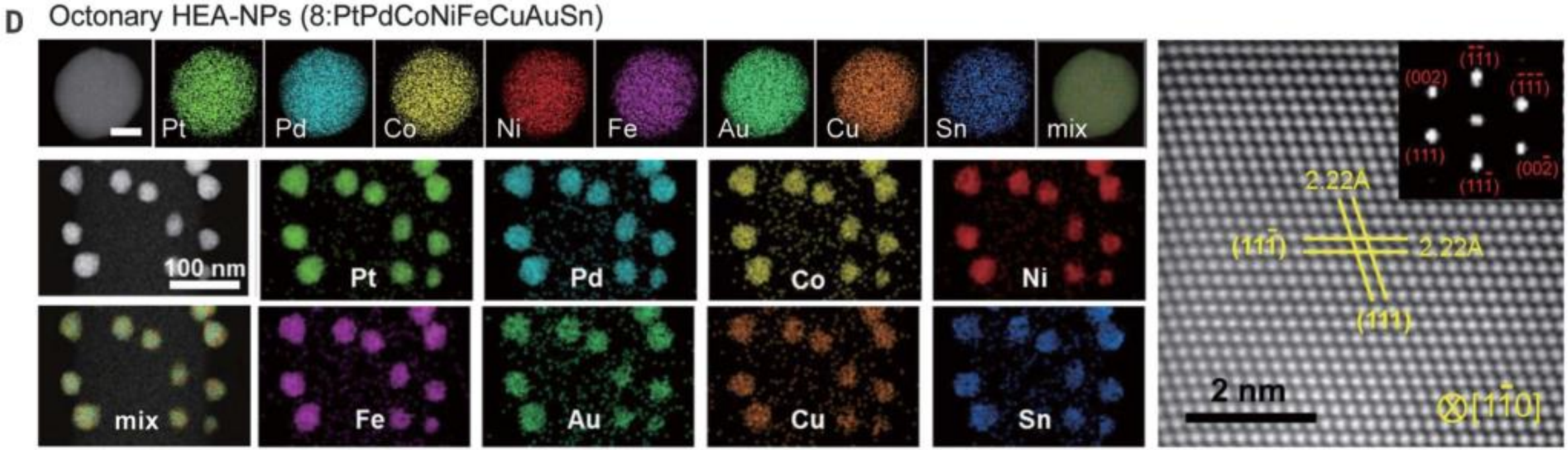

Fig. 2 (contd.) (D) Individual and low-magnification elemental maps (left) and a high-resolution HAADF-STEM image with fast Fourier transform analysis (right) of octonary (PtPdCoNiFeCuAuSn) HEA-NPs, showing solid solutions with an fcc structure. The low-magnification elemental maps verify the structural and compositional uniformity of the HEA-NPs. Scale bar, 10 nm.

Results
Particle Dispersion Mechanism for the CTS Process

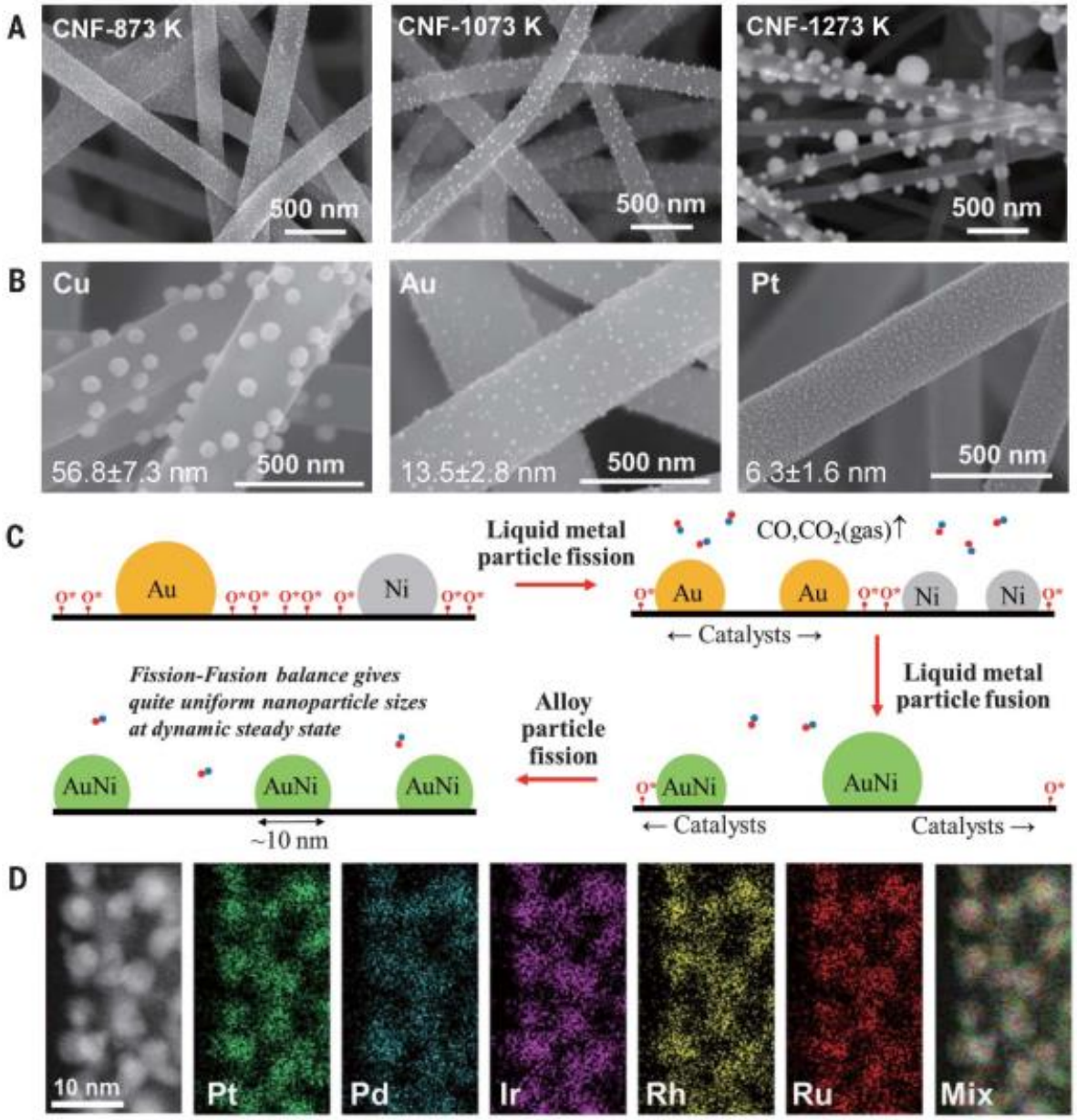

Fig. 3. Particle dispersion mechanism for the CTS process. (A) SEM images of synthesized AuNi nanoparticles on CNFs carbonized at different temperatures: 873, 1073, and 1273 K. A higher carbonization temperature leads to higher crystallinity and lower defect concentrations within the carbon support, which affects particle size and dispersion. (B) SEM images of Cu, Au, and Pt particle distributions synthesized on identical CNF supports via the same CTS process. The higher catalytic activities of the metal species (Au and Pt) lead to smaller nanoparticles and more uniform distributions. (C) An illustration of the catalysis-driven particle fission/fusion mechanism to synthesize uniformly dispersed HEA-NPs. (D) HAADF image and elemental maps of ultrafine and well-dispersed quinary HEA-NPs (PtPdIrRhRu) on CO2-activated CNFs. A narrow size distribution is achieved by increasing the support's surface defect concentration through CO2 activation, as well as employing metal species with high catalytic activities.

Results
Kinetic Control Over NP Formation

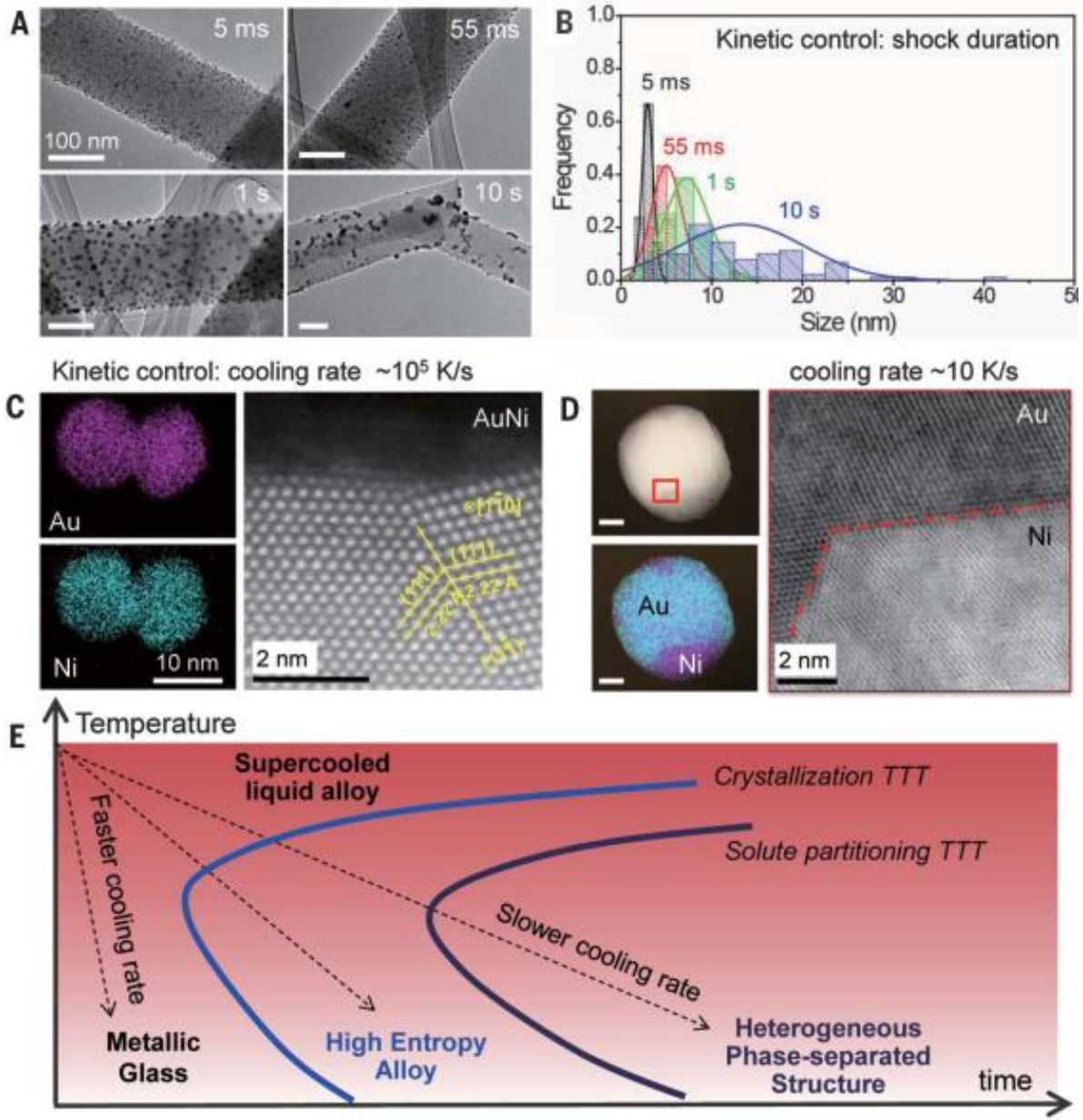

Fig. 4. Kinetic control over nanoparticle formation. (A) TEM images displaying the particle size and dispersity at various thermal shock durations (5 ms, 55 ms, 1 s, and 10 s). Scale bars, 100 nm. (B) Particle size distribution of PtNi nanoparticles on CNFs. (C and D) Cooling rate–dependent AuNi nanostructures determined by elemental maps, HAADF, and ABF images. Ultrafast cooling rates (~10^5 K/s) enable the formation of solid-solution nanoparticles, whereas slower rates (~10 K/s) tend to induce phase separation. Scale bar, 10 nm. (E) Time-temperature-transformation (TTT) diagram showing the kinetic formation of metallic glass, HEA, and phase-separated structures, respectively, as a function of cooling rate

Results
Catalytic Performance of Quinary HEA-NPs in Ammonia Oxidation

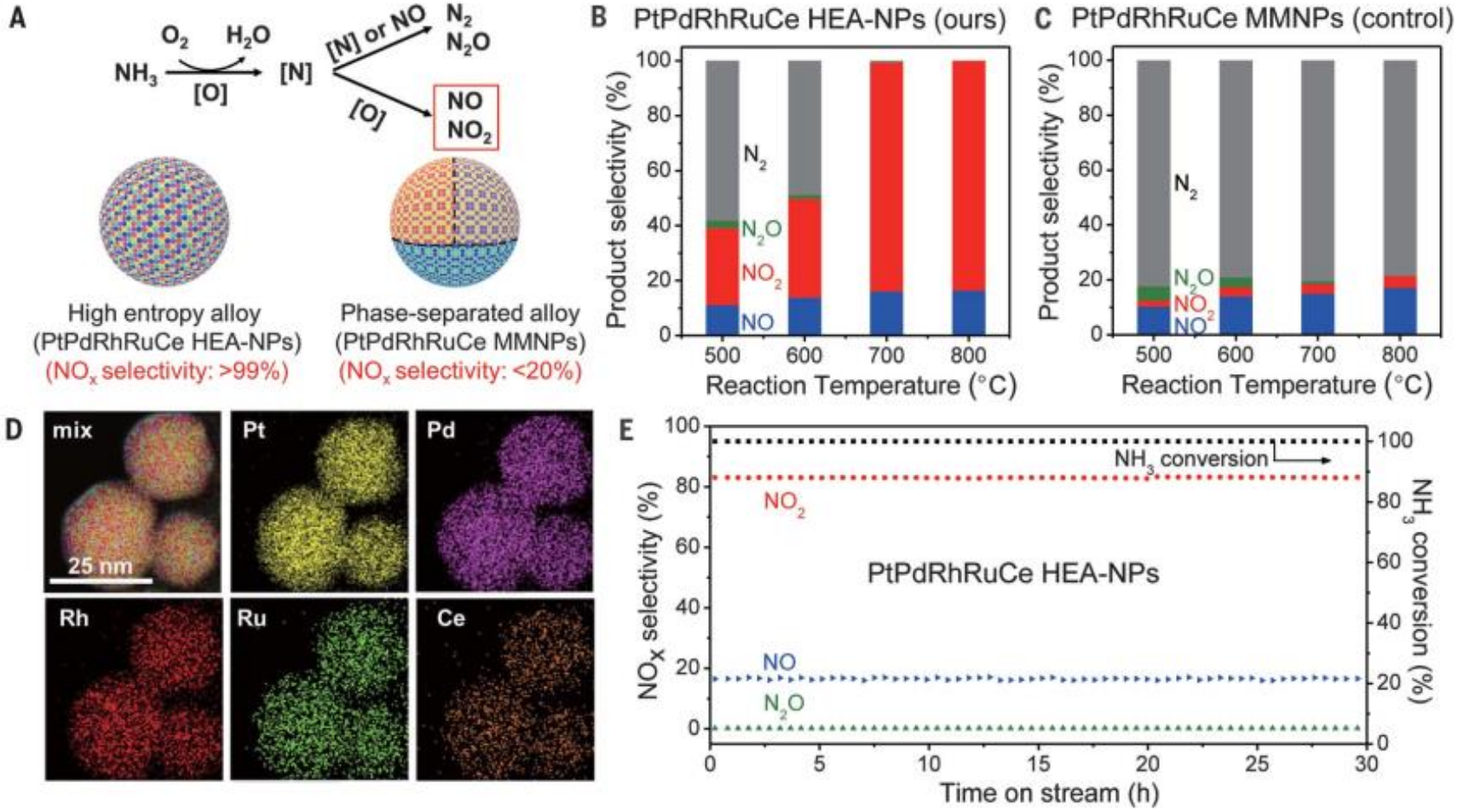

Fig. 5. Catalytic performance of quinary HEA-NPs (PtPdRhRuCe) for ammonia oxidation. (A) Reaction scheme for the ammonia oxidation process as well as the structural and performance differences between the PtPdRhRuCe HEA-NPs synthesized by CTS and the control sample (PtPdRhRuCe MMNPs) by wet impregnation. (B and C) Temperature-dependent product distribution and conversion of NH_3 for PtPdRhRuCe HEA-NPs and PtPdRhRuCe MMNPs, respectively. (D) STEM elemental maps for PtPdRhRuCe HEA-NPs. (E) The time-dependent catalytic performance of PtPdRhRuCe HEA-NPs at 700°C.

Conclusions

- Immiscible elements are alloyed into single-phase nanoparticles on carbon supports with the following features:

  (i) high-entropy mixing, (ii) non-equilibrium processing, and (iii) uniform dispersion

- This synthetic technique also provides

  (i) generality, (ii) tunability, and (iii) potential scalability